

ornl

**OAK RIDGE
NATIONAL
LABORATORY**

MARTIN MARIETTA



3 4456 0064787 9

ORNL/TM-9703

Effect of Electric Fields and Fluctuations on Confinement in a Bumpy Torus

S. Hirce
J. C. Glowienka
D. L. Hillis
J. B. Wilgen
G. L. Chen
J. A. Cobble

A. M. El-Nadi
J. R. Goyer
L. Solensten
W. H. Casson
O. E. Hankins
B. H. Quon

OPERATED BY
MARTIN MARIETTA ENERGY SYSTEMS, INC.
FOR THE UNITED STATES
DEPARTMENT OF ENERGY

OAK RIDGE NATIONAL LABORATORY
CENTRAL RESEARCH LIBRARY
CIRCULATION SECTION
EAST ROOM 111
LIBRARY LOAN COPY
DO NOT TRANSFER TO ANOTHER PERSON
If you wish someone else to see this
report, send in some with report and
the library will arrange a loan.

Printed in the United States of America. Available from:
National Technical Information Service
U.S. Department of Commerce
5285 Port Royal Road, Springfield, Virginia 22161
NTIS price codes—Printed Copy: 13—Microfilm: 14

This report was prepared as an account of work sponsored by an agency of the United States Government. Neither the United States Government nor any agency thereof, nor any of their employees, makes any warranty, expressed or implied, or assumes any legal liability or responsibility for the accuracy or completeness or usefulness of any information, apparatus, product, or process disclosed, or represents that its use would not infringe privately owned rights. Reference herein to any specific commercial product, process, or service by trade name, trademark, manufacturer, or otherwise, does not necessarily constitute or imply its endorsement, recommendation, or favoring by the United States Government or any agency thereof. The views and opinions of authors expressed herein do not necessarily state or reflect those of the United States Government or any agency thereof.

Fusion Energy Division

EFFECT OF ELECTRIC FIELDS AND FLUCTUATIONS
ON CONFINEMENT IN A BUMPY TORUS

S. Hiroe
J. C. Glowienka
D. L. Hillis
J. B. Wilgen
G. L. Chen
J. A. Cobble*

A. M. El-Nadi^{+ 2}
J. R. Goyer^{† 3}
L. Solensten^{‡ 3}
W. H. Casson^{§ 4}
O. E. Hankins^{¶ 5}
B. H. Quon^{# 4}

*Present address: Los Alamos National Laboratory, Los Alamos, New Mexico

+Present address: Cairo University, Giza, Egypt

†Rensselaer Polytechnic Institute, Troy, New York

‡The University of Tennessee, Knoxville

¶University of North Carolina at Raleigh

#JAYCOR, Torrance, California

Date Published: June 1986

Prepared by the
OAK RIDGE NATIONAL LABORATORY
Oak Ridge, Tennessee 37831
operated by
MARTIN MARIETTA ENERGY SYSTEMS, INC.
for the
U. S. DEPARTMENT OF ENERGY
under Contract No. DE-AC05-84OR21400



3 4456 0064787 9

CONTENTS

	Page
ABSTRACT	v
I. INTRODUCTION	1
II. EXPERIMENTAL SETUP	2
III. ROLE OF POTENTIAL IN CONFINEMENT	6
A. Plasma Parameters	6
B. Equilibrium Potential Contours	8
C. Dependence of Potential on Plasma Parameters	17
IV. EFFECT OF FLUCTUATIONS ON THE PLASMA	19
A. Density Fluctuations	19
B. Interchange Stability Criterion	24
C. Discussion of the Stability of the Interchange Mode (Coherent Mode)	26
D. Correlation of Background Noise with Plasma Parameters	28
V. SCALING OF PLASMA PARAMETERS	31
VI. CONCLUSION	34
VII. ACKNOWLEDGMENTS	35
REFERENCES	37

ABSTRACT

In order to understand the relationships between confinement and space potential (electric field) and between confinement and density fluctuations, plasma parameters in the ELMO Bumpy Torus Scale (EBT-S) have been measured systematically for a wide range of operating conditions. Present EBT plasma parameters do not show a strong dependence on the potential profile, but rather exhibit a correlation with the fluctuations. The plasma pressure profile is found to be consistent with the profile anticipated on the basis of the flute stability criterion for a marginally stable plasma. For a heating power of 100 kW, the stored energy density is found to be restricted to the range between 4.5×10^{13} eV-cm⁻³ and 7×10^{13} eV-cm⁻³. The lower limit remains constant regardless of heating power and pertains to plasmas lacking an equilibrium and/or stability. The upper limit increases with heating power and is found to result from the onset of instabilities. In between the two limits is a plasma that is in an equilibrium state and is marginally stable. Operational trajectories exist that take the EBT plasma from one limit to the other.

I. INTRODUCTION

A bumpy torus with high-beta, hot-electron rings generated by electron cyclotron heating (ECH) may be promising as a steady-state plasma device that embodies the ELMO Bumpy Torus (EBT) concept.^{1,2} The hot electron rings can reverse the gradient of $\oint d\ell/B$ if the ring beta is high enough, thereby providing gross magnetohydrodynamic (MHD) stability.³

Early experimental results from the EBT experiment at Oak Ridge National Laboratory indicated that a stable mode of operation designated the T-mode was achieved simultaneously with the formation of the hot electron rings. In the T-mode, a negative potential well was observed,⁴ and plasma parameters appeared to follow neoclassical scaling.^{2,5}

Recent experimental investigations in EBT have found that nested closed potential contours are present in the T-mode, but that the high-pressure mode designated the C-mode is characterized by the typical nonequilibrium of a simple torus with horizontal potential contours⁶ formed by charge separation due to vertical drifts. In spite of these substantial differences in potential between C-mode and T-mode, the energy density and, hence, the plasma confinement for these two cases differ by only a factor of two. This suggests the first issue addressed in this paper: the relationship between the electric field and plasma confinement. The data presented demonstrate that, in contrast to the expectations of neoclassical theory,² confinement depends only weakly on the electric field in the EBT device.

The second issue to be explored is the relationship between plasma confinement and stability of the plasma. Recent measurements^{7,8} of the hot electron rings indicate that beta is not likely to exceed 10%, which is insufficient to reverse the gradient of $\oint d\ell/B$. In view of these observations, instability activity (fluctuations) must be regarded as a likely contributor to

the electron transport. Measurements of fluctuations in the electron density are presented and compared with plasma parameters. It is shown that there is a correlation of fluctuations with degradation of confinement. Low-frequency fluctuations have previously been measured and identified by Komori.⁹ In this paper, the relationship between the plasma parameters (i.e., the pressure profile and the energy density) and the fluctuations is developed on the basis of Komori's identification of the instabilities. The measured plasma pressure profile is compared with a profile governed by the flute stability criterion,¹⁰ which is expressed as $\delta[\ln(pU^\gamma)] > 0$, where p is the plasma pressure, $U = \oint d\ell/B$, and γ is the specific heat ratio. The plasma is found to be marginally stable due to the lack of reversal of U in the present configuration.

On the basis of these results, it is questionable that confinement is neoclassical. It is therefore of interest to examine the scaling of the basic plasma parameters. In general, it is found that there is an inverse relationship between n_e and T_e , such that the product $n_e T_e$ is a constant. For a heating power of 100 kW, the stored energy density is found to be restricted to the range between 4.5×10^{13} eV-cm⁻³ and 7×10^{13} eV-cm⁻³. Using the nonequilibrium C-mode as a base case, stored energy is improved by a factor of two in the marginally stable T-mode.

This paper is organized as follows: the experimental setup is described in Sec. II. The effect of electric field on confinement is presented in Sec. III, and the effects of fluctuations on the plasma are discussed in Sec. IV. The scaling relation is presented in Sec. V. The conclusion is presented in Sec. VI.

II. EXPERIMENTAL SETUP

The EBT device¹¹ consists of 24 cavities that are placed between canted mirror coils and are connected toroidally as shown schematically in Fig. 1.

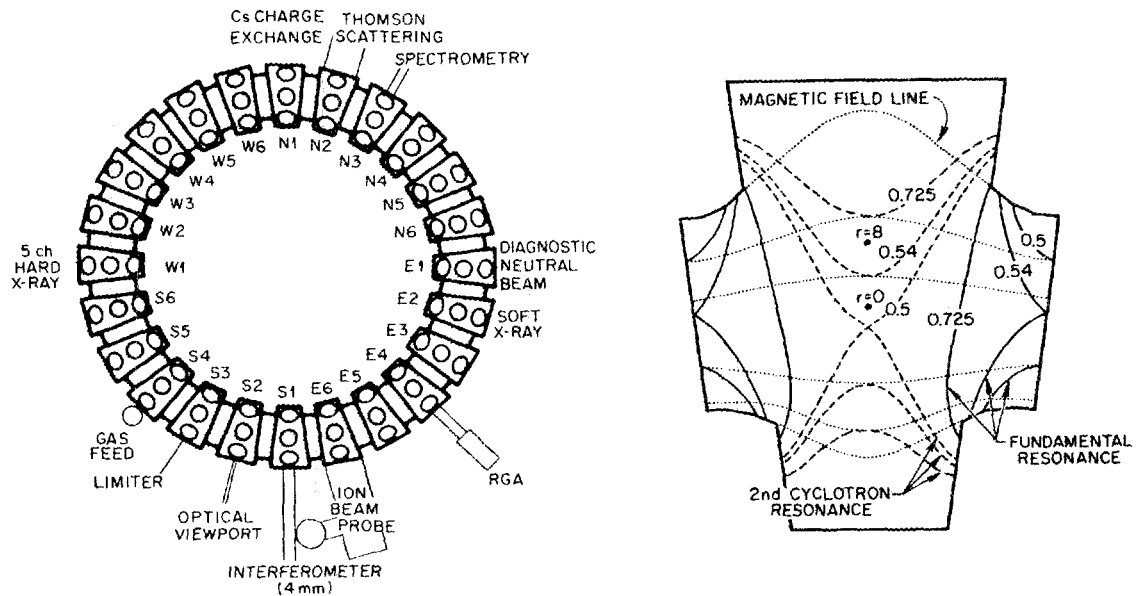


Fig. 1. At left, locations of diagnostics used in this experiment; right half, the fundamental (solid lines) and second electron cyclotron resonance zones (broken lines) for 28-GHz microwave heating. The numbers indicate the magnetic field strength (in T) at the center of the midplane for the different coil currents. Several magnetic field lines (dotted) are displayed. The radial points where n_e and T_e are measured by Thomson scattering are also shown by $r = 0$ and $r = 8$ cm.

The initial microwave frequency was 18 GHz, and the machine is called EBT-I when operated at this level. Klystron output power up to 60 kW is available. EBT-Scale (EBT-S) is usually operated in a steady state with plasma produced by electron cyclotron resonance heating (ECRH) using a 28-GHz gyrotron. Except for a few examples, EBT-S data are primarily discussed here. Gyrotron output power up to 200 kW is available, but generally EBT is operated at 100 kW.

The magnetic field strength can be varied up to 0.725 T on the midplane. Normally, EBT-S is operated at $B = 0.725$ T. (In this paper, values for B indicate the magnetic field strength on the magnetic axis at the midplane.) Let us consider the movement of the electron cyclotron resonance zone for 28 GHz caused by changing the magnetic field strength. At $B = 0.725$ T, the fundamental heating zone is at $z \approx 10$ cm along the toroidal direction, where $z = 0$ is at the midplane, as shown on the right side of Fig. 1. The radius of the second cyclotron resonance, where the hot electron annulus is expected to form, is $r = 12$ cm. When the magnetic field is reduced from 0.725 T, the fundamental resonance zone moves toward the mirror throat and reaches $z \approx 20$ cm [$= (2\pi R/24)/2$] at $B = 0.54$ T, where $R = 150$ cm is the major radius. The second cyclotron resonance zone also moves inward as B is reduced and crosses the magnetic axis when $B = 0.5$ T.

The diagnostics used in this experiment are also shown in Fig. 1. The line integral density is measured with a 4-mm interferometer. A continuing effort has been made by a group from Rensselaer Polytechnic Institute (RPI) to obtain electrostatic potentials in EBT by means of a cesium heavy-ion beam probe. Recently,¹² this probe has been used to measure two-dimensional equipotential contours, thus providing the ability to investigate the effect of electric field on confinement. A Thomson scattering system¹³ is used to

measure the bulk electron density n_e and the electron temperature T_e . Due to the low density ($n_e < 10^{12} \text{ cm}^{-3}$), the signal-to-noise ratio is not good enough to measure n_e and T_e in one shot. In general, the sum of 10 shots is analyzed. Thomson scattering is used to obtain n_e and T_e profiles for a few representative cases; otherwise, the radial profile is deduced from Thomson scattering data measured at two different radial positions, $r = 0 \text{ cm}$ and 8 cm . Note that the position of $r = 8 \text{ cm}$ is outside the second cyclotron resonance (expected hot electron ring radius) when the magnetic field strength is below 0.64 T .

The line integral density fluctuations are measured from the direct output signal of the crystal detector in the 4-mm interferometer system. The frequency response (0-500 kHz) is high enough to consider drift waves, interchange modes, and other relevant instabilities. The measurement is primarily sensitive to poloidal fluctuations with wavelengths larger than 2-3 cm. In some cases, such as flutes with odd mode number, cancellation effects can reduce the sensitivity. Since the experimentally observed range of mode numbers is less than 20, corresponding to wavelengths greater than 3 cm, the sensitivity reduction is qualitatively small.

In order to understand the physical mechanisms governing confinement in EBT, the plasma parameters have been measured systematically for a wide range of operating conditions. The independently variable EBT parameters are the microwave power P_μ , the hydrogen pressure p_0 , and the magnetic field B . Most of the data presented here are taken from scans of the magnetic field. The primary reason for this choice is the observation that, as the magnetic field is reduced from the normal value, the potential well changes smoothly from the negative well characteristic of T-mode to a positive potential hill, thus permitting an evaluation of the effects of the electric field on

confinement. A secondary reason comes from the expectation that if the hot electron annulus determines the core-surface plasma boundary, the plasma parameters radially outside the annulus should be different from those radially inside the annulus, providing the ability to discuss the stability boundary defined by the hot electron annulus.

It is also of interest to examine other cases in which the potential is modified but the magnetic field is not. This is achieved by varying the pressure, by introducing magnetic field errors, and by operating with a single movable limiter or a toroidal array of fixed limiters (ring modifiers and ring killers¹⁴). For organizational clarity in the following sections, data obtained from magnetic field scans are treated first and are followed by other cases of special interest.

III. ROLE OF POTENTIAL IN CONFINEMENT

A. Plasma Parameters

In Fig. 2 the line integral plasma density ($n_e \ell$) is plotted against the ambient pressure (p_0) for different values of the external magnetic field B . During normal operation ($B = 0.725$ T), one can define three operational modes. The C-mode appears during high-pressure operation and shows the monotonic decrease of $n_e \ell$ as p_0 is reduced. At $p_0 = 1.3 \times 10^{-5}$ Torr, $n_e \ell$ starts to increase. This operating point, called the T-C transition, is where nested potential contours⁶ begin to form. At $p_0 \approx 9 \times 10^{-6}$ Torr, $n_e \ell$ starts to decrease again (called the "knee" point). Below $p_0 = 9 \times 10^{-6}$ Torr, $n_e \ell$ continues to decrease up to the T-M transition as p_0 is reduced further. The plasma is said to be in the T-mode between the T-C transition and the T-M transition where the potential contours are nested. Near the T-M transition, hot electron

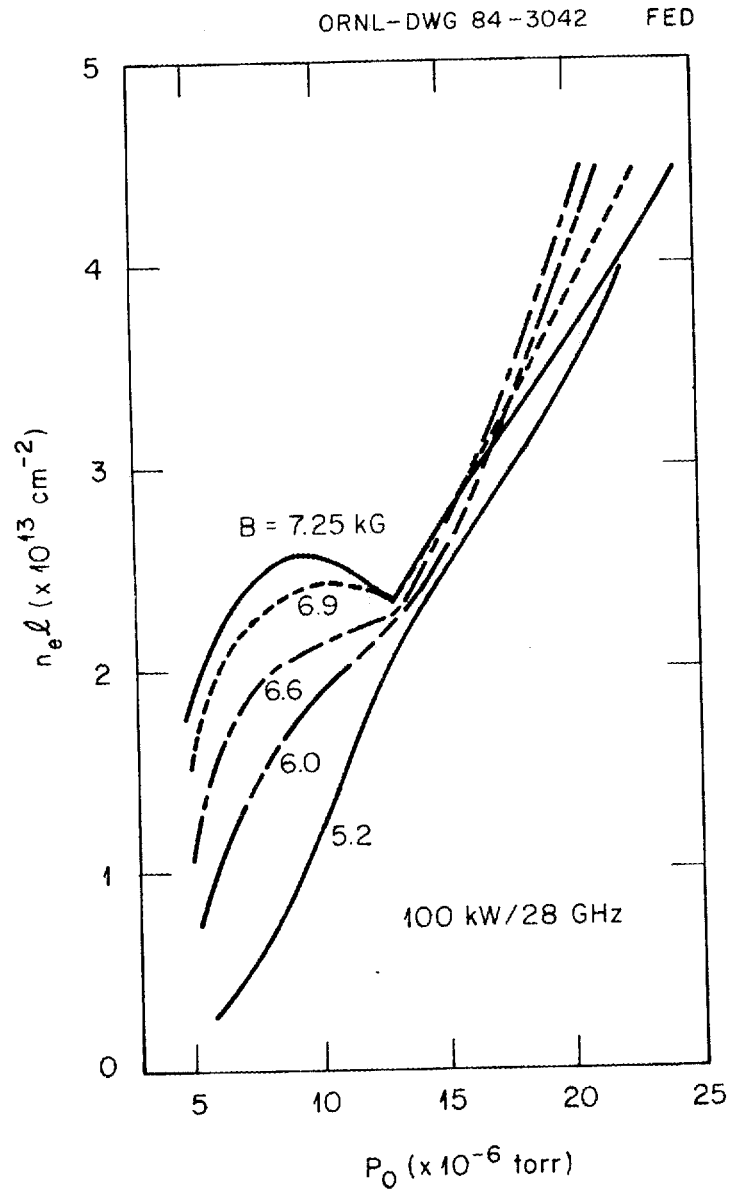


Fig. 2. Line integral densities vs ambient pressure for different magnetic field strengths.

instabilities¹⁵ destroy the plasma because of a large hot electron-to-background ion density ratio.

When the magnetic field is reduced, the T-mode operation window becomes narrower, and $n_e \ell$ in T-mode decreases, while $n_e \ell$ in C-mode does not change markedly. When B is reduced further, the increment of $n_e \ell$ in the T-mode is also reduced. Below $B = 0.58$ T, the T-mode window completely disappears, and the line integral density ($n_e \ell$) decreases monotonically over the whole pressure range from high pressure to low pressure.

The electron temperature (T_e) and density (n_e) at $r = 0$ and 8 cm are plotted in Fig. 3 as a function of B by holding the power and pressure constant at $P_\mu = 100$ kW and $p_0 = 8 \times 10^{-6}$ Torr. The electron density at $r = 0$ and 8 cm increases as the magnetic field increases. This implies that the density profile remains roughly constant but that the density itself increases as B increases.

The electron temperature at $r = 0$ cm is a decreasing function of B. The electron temperature at $r = 8$ cm shows large error bars concomitant with low density ($n_e \sim 2 \times 10^{11} \text{ cm}^{-3}$). Within the limit of this scattering of data, T_e may be implied to remain almost constant with B. It is important to point out that the T_e profile of the bulk electrons is hollow for operation at high magnetic field.

B. Equilibrium Potential Contours

The potential structure (details of the shape of the potential contours from which the electric field is obtained) plays an important role in the equilibrium and confinement for a device without a rotational transform.^{6,16,17} The potential contours are presented for the six cases shown in Fig. 4. Figure 4(a) shows an equipotential contour plot for the normal EBT-S operation.

ORNL-DWG 84-3054R2 FED

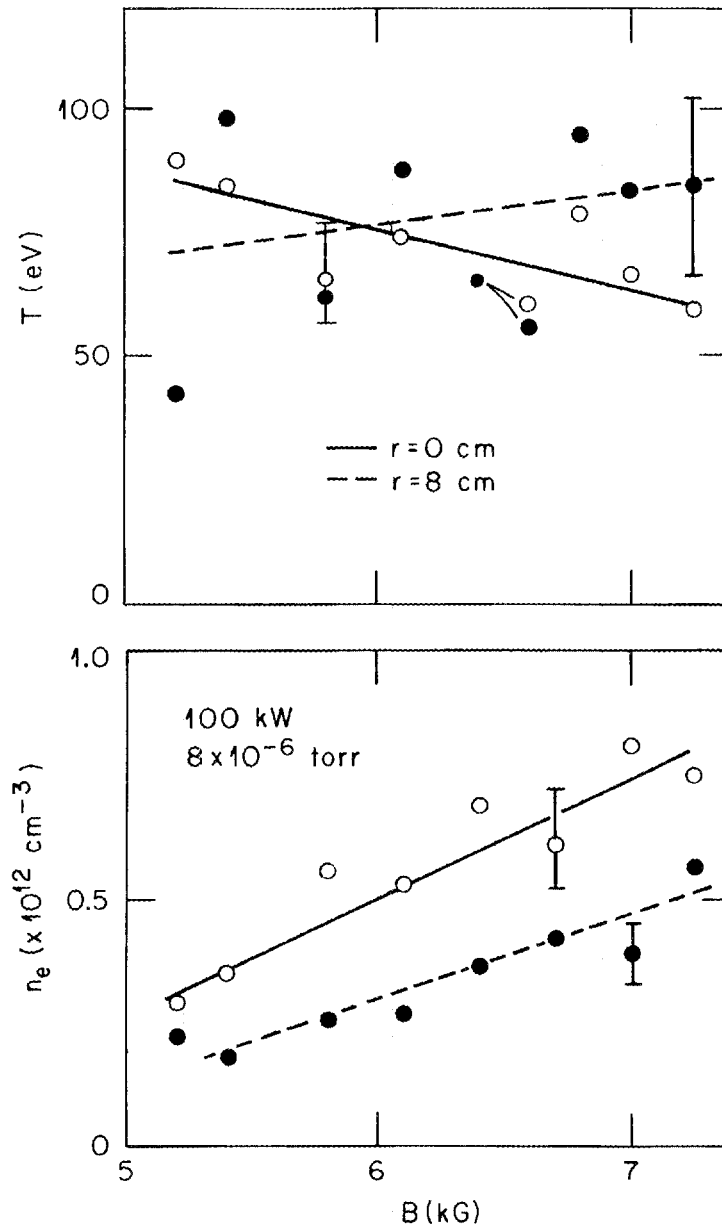


Fig. 3. The electron density and temperature, measured by Thomson scattering at $r = 0$ (open circles) and 8 cm (closed circles), vs magnetic field strength. The heating power is 100 kW, and the ambient pressure is 8×10^{-6} Torr. Below $B = 0.64$ T, the second cyclotron resonance zone moves inside $r = 8$ cm.

ORNL-DWG 84-3734 FED
T-MODE

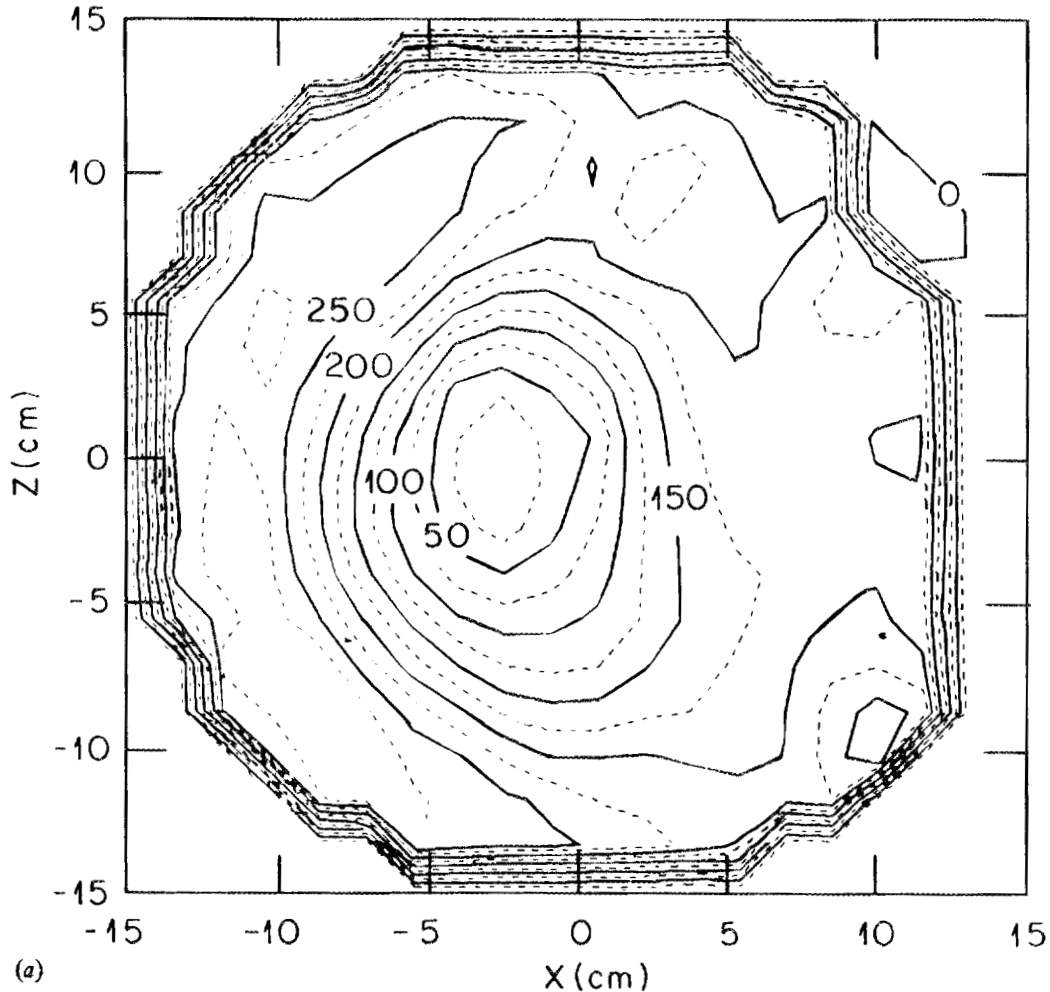


Fig. 4. Two-dimensional equipotential contours for various plasma conditions. The heating power is 100 kW. (a) Typical T-mode at $B = 0.725$ T, $p_0 = 8 \times 10^{-6}$ Torr, and $r_{\text{ring}} \sim 11.5$ cm; (b) $B = 0.58$ T, $p_0 = 8 \times 10^{-6}$ Torr, and $r_{\text{ring}} \sim 8$ cm; (c) $B = 0.52$ T, $p_0 = 8 \times 10^{-6}$ Torr, and $r_{\text{ring}} \sim 4$ cm; (d) no error field correction ($\delta B/B_0 \sim 10^{-3}$); (e) limiter positioned about 1 cm inside the second cyclotron resonance, $B = 0.725$ T, and $p_0 = 8 \times 10^{-6}$ Torr; (f) C-mode at $B = 0.725$ T and $p_0 = 2 \times 10^{-5}$ Torr (not in equilibrium).

ORNL-DWG 84-3729 FED

B = 5.8 kG

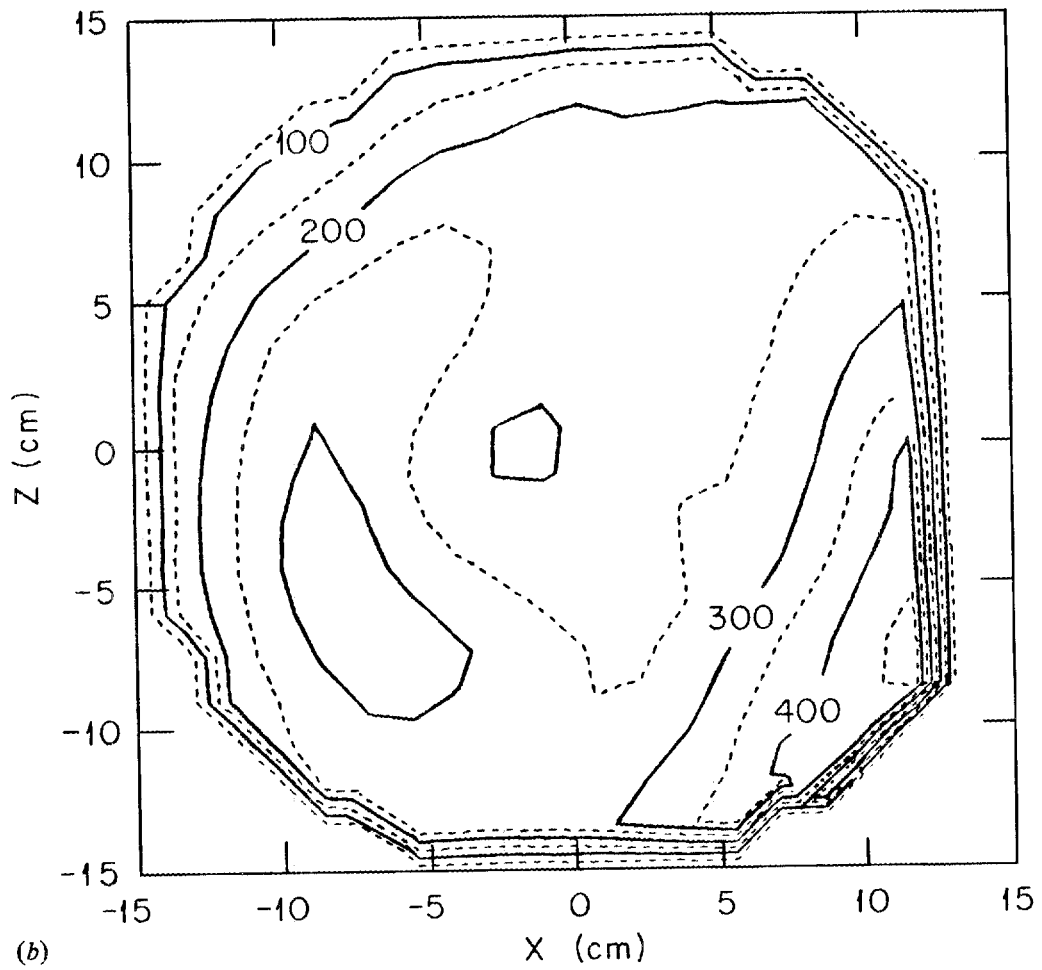


Fig. 4 (continued)

ORNL-DWG 84-3730 FED

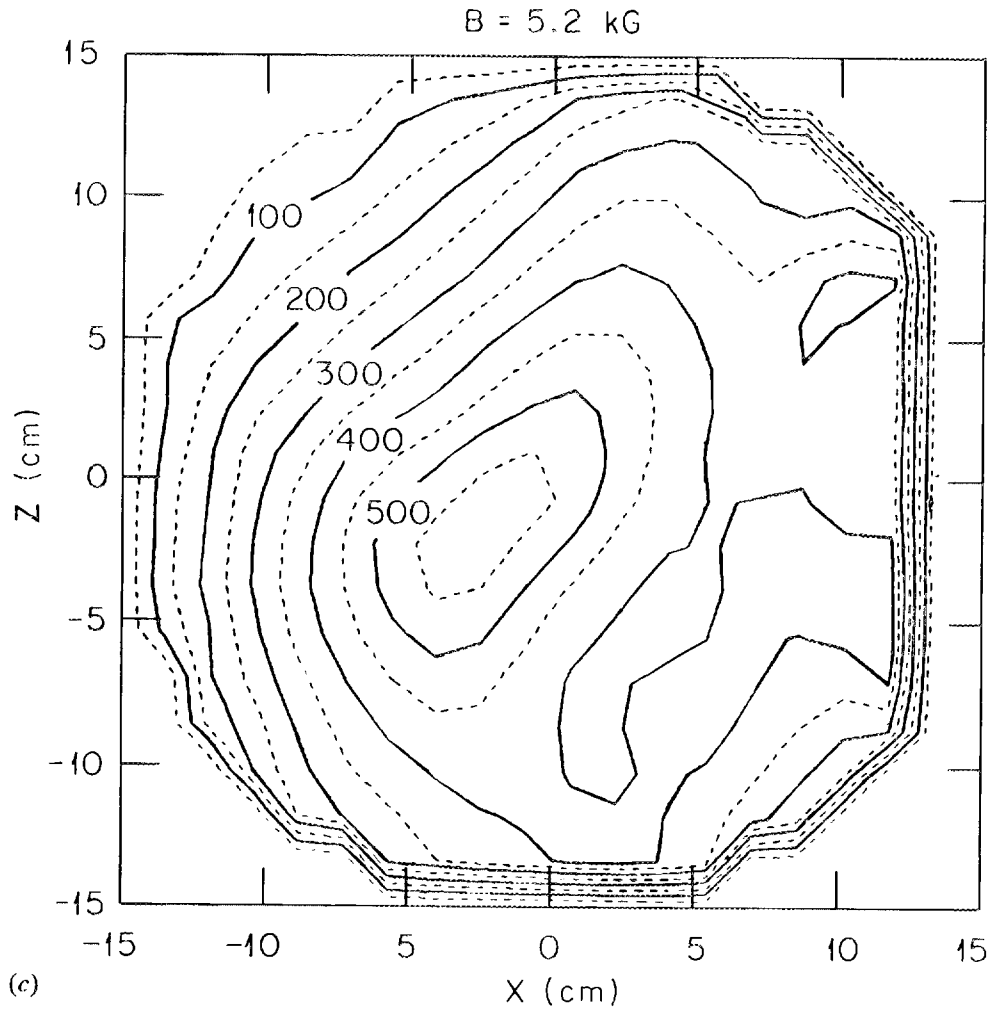
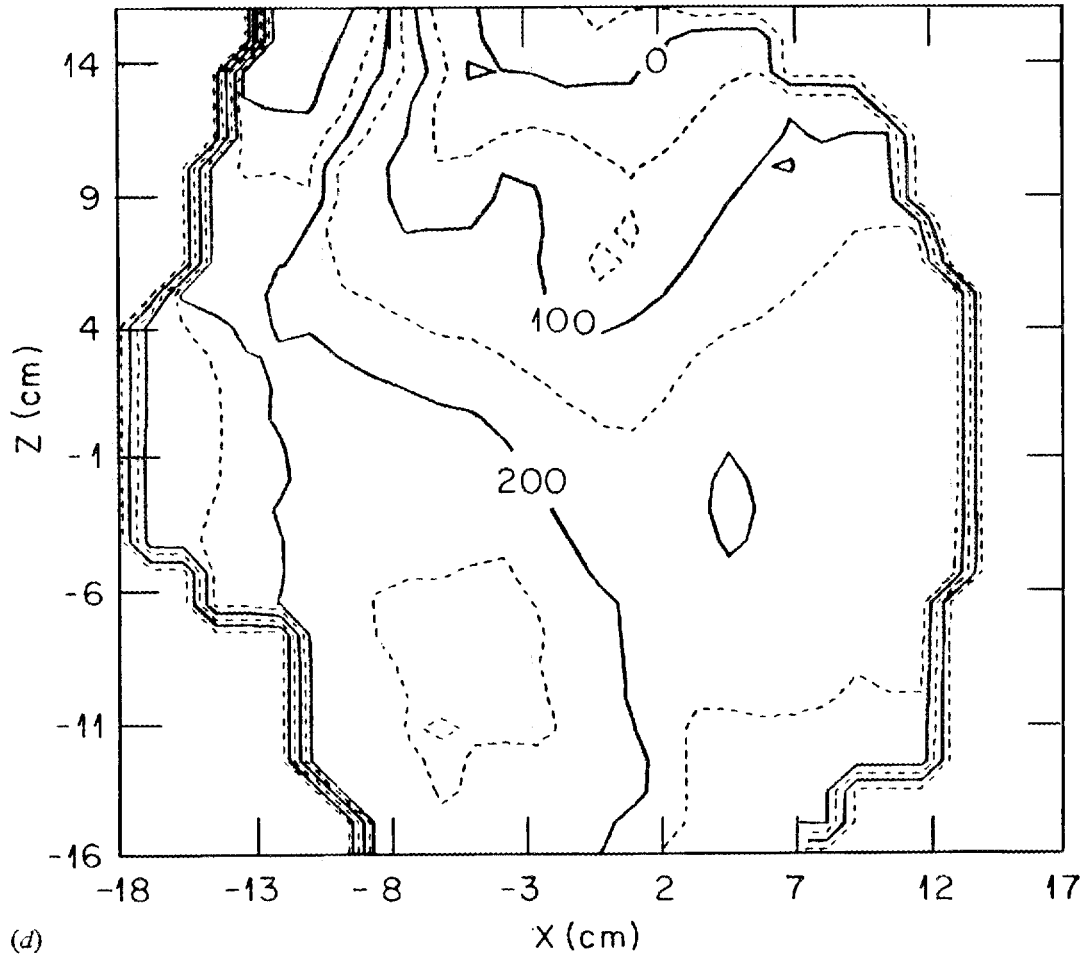


Fig. 4 (continued)

ORNL-DWG 84-3728 FED

ERROR FIELD



(d)

Fig. 4 (continued)

ORNL-DWG 84-3732A FED

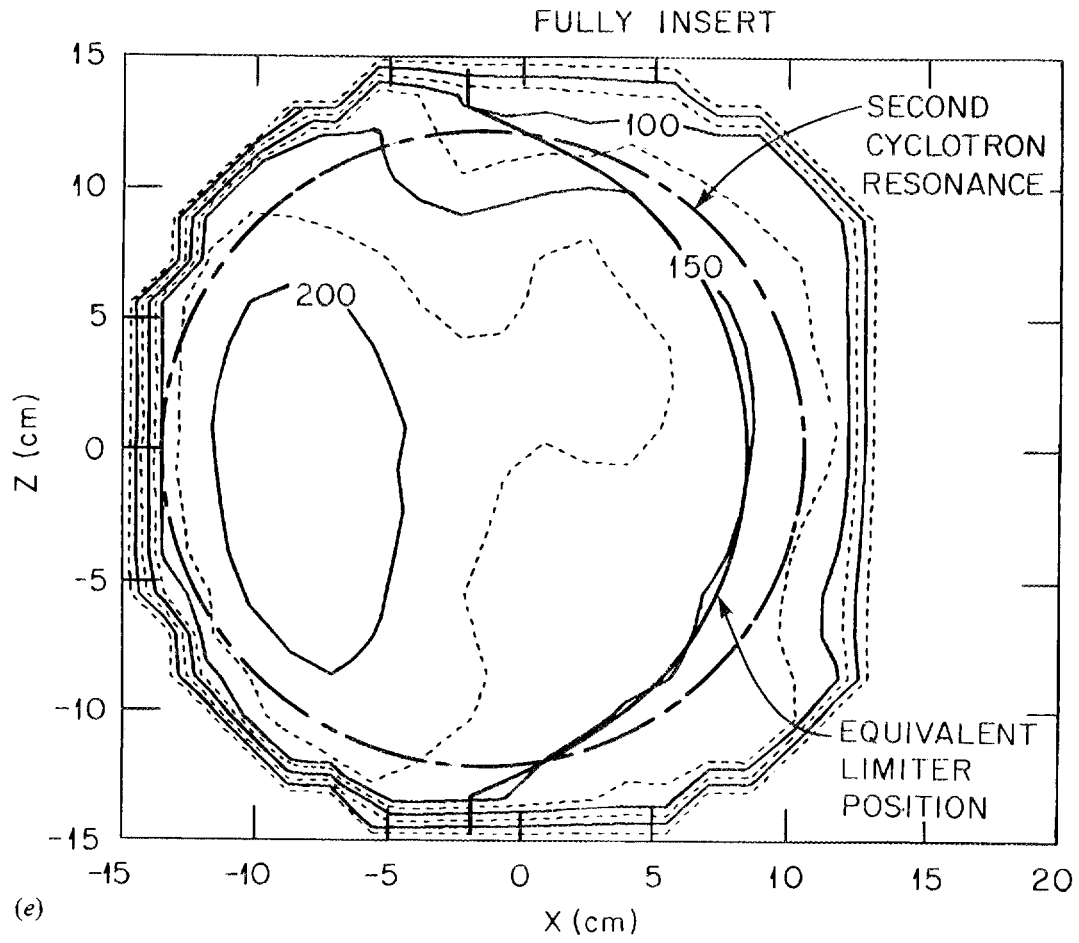


Fig. 4 (continued)

ORNL-DWG 84-3733 FED
C-MODE

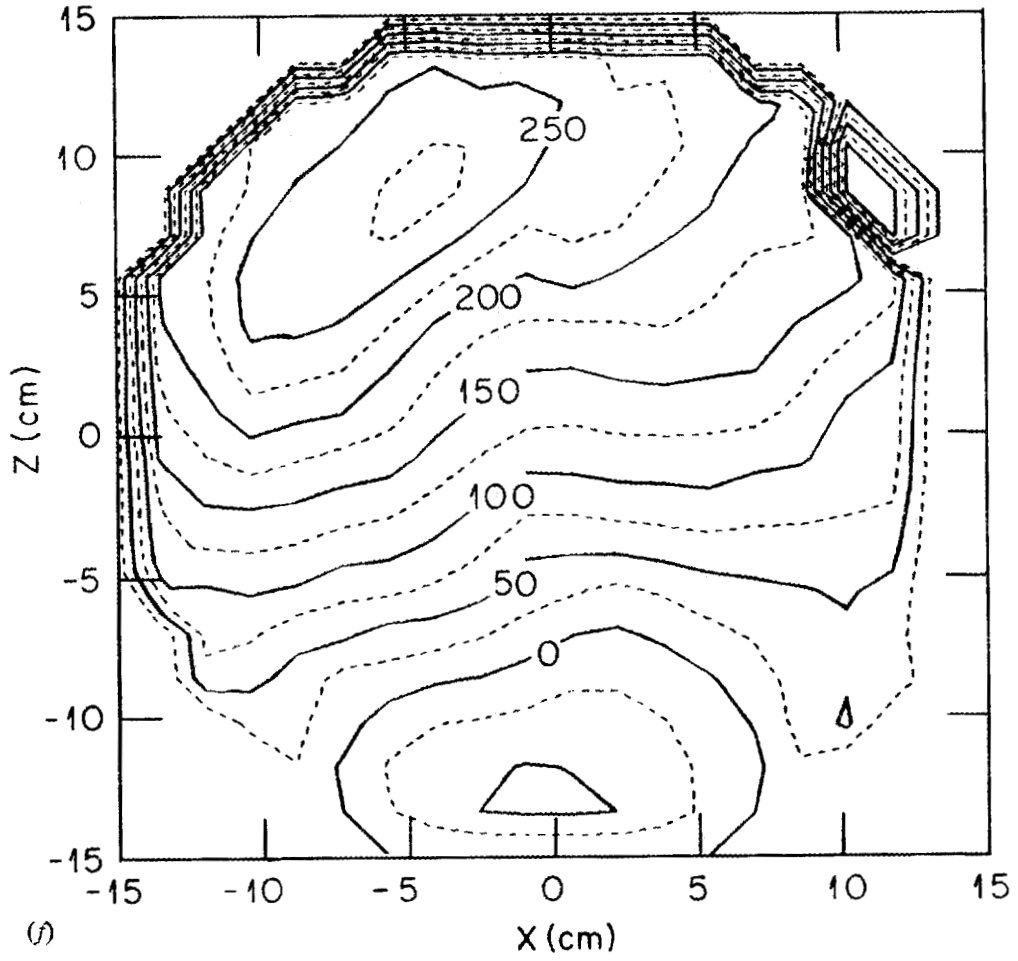


Fig. 4 (continued)

Typically, nested, closed equipotential contours are found in the central region ($r < 5\text{--}7$ cm). The central potential is negative (potential well) with respect to the potential maximum found in the region of the ring ($r = 12$ cm at $B = 0.725$ T). A net potential well depth of 200 to 500 V is found under various EBT-S operating conditions.

As the magnetic field is decreased, the positive potential hill near the edge of the potential well moves inward, following the location of the second harmonic resonance heating¹ (see Fig. 1). The potential well depth also becomes shallower as the magnetic field is decreased. The general shape of the potential well does not change significantly until the second harmonic resonance region is close to the magnetic axis. When this happens, the space potential well disappears, and a positive potential hill is observed everywhere, as shown in Fig. 4(b), where a very weak electric field is found in the confinement area. A large positive potential hill near the magnetic axis is observed at $B = 0.52$ T, where the second harmonic heating zone actually moves in toward the magnetic axis, as shown in Fig. 4(c).

The plasma potential can be strongly affected by introducing external magnetic error fields. With an error field $\delta B/B > 5 \times 10^{-4}$, the potential well in the T-mode operation is replaced by a simple potential structure where no nested potential contours are found, as shown in Fig. 4(d).

Another interesting potential profile is found when the movable limiter is set just inside the hot electron annulus, as shown in Fig. 4(e). The potential well is replaced by a positive potential hill. Even when the limiter is fully inserted and intercepts a large amount of the plasma region, the potential contours are the same as those in Fig. 4(e).

The potential structure in the case of a nonequilibrium state is shown in Fig. 4(f), where the plasma is in the C-mode. The electric field is directed

vertically, resulting from the charge-dependent vertical drift due to the toroidal effect. This is the expected potential contour for the simple torus with no rotational transform. (A detailed discussion of the last two cases is presented in Ref. 6.)

C. Dependence of Potential on Plasma Parameters

An important question to be answered is: Does the electrostatic potential play an important role on EBT confinement? The plasma parameters are listed in Table I for the different potential shapes and the values of the electric field strength obtained from $-\partial\phi/\partial r$ at $r \sim 5$ cm (horizontally inside). Case 1 in this table corresponds to Fig. 4(a), case 2 to Fig. 4(b), case 3 to Fig. 4(c), case 5 to Fig. 4(f), case 6 to Fig. 4(d), and case 10 to Fig. 4(e).

It is clear that the stored energy densities $W_e = 3/2(n_e T_e)$ are within 50% of each other in the same category (for example, magnetic field scan). The insensitivity of the stored energy to the radial electric field E indicates that the energy confinement is not consistent with the neoclassical scaling² of $(E/T_e)^2$ in the collisionless regime. For example, the ratio of $(E/T_e)^2$ for case 6 and for case 7 is more than 10, but the ratio of stored energy values for the two cases is almost 1.

Another interesting result is shown in cases 1 through 3. Following neoclassical theory, the plasma in case 2 is in the collisional regime, and the other two cases are in the collisionless regime because the precession frequency due to the $E \times B$ drift is approximately 50 times higher than that of poloidal ∇B drift. However, the difference in stored energies is within a factor of 50%. Moreover, the stored energy of the plasma in an equilibrium state (case 4) is twice as large as the energy density of the plasma in a

Table I. The electron density, temperatures^a, electric field strength, and potential structure for the various experimental arrangements on EBT

Case		Potential shape	E (V/cm)	n _e (10 ¹¹ cm ⁻³)	T _e (eV)	(n _e T _e) ratio	
1	Magnetic field scan	7.25 kG	Well	>30	8.3	60	1.0
2		5.8 kG	No closed contour	≪10	5.8	62	0.72
3		5.2 kG	Hill	>30	3.0	90	0.54
4	Pressure scan	Low p ₀	Well	~50	6.0	90	1.0
5.		High p ₀	No equilibrium	~10	6.0	50	0.56
6.	Error field	No correction current	No closed contour	≪10	8.4	67	1.15
7		Correction current	Well	30	9.8	50	1.0
8	Limiter scan	Out	Well	30	13.6	113	1.0
9		Just outside ring	Symmetric well	>30	12.9	148	1.24
10		Just inside ring	No closed contour	0	11.1	100	0.72
11		Fully inserted	No closed contour	0	11.7	97	0.74

^aThe electron temperatures for cases 8-11 are approximately 50% higher than those for the other cases because of an inability to accurately quantify the background light level in the limiter scans.

nonequilibrium state (case 5). From these discussions, it is reasonable to conclude that transport in the plasmas of the EBT device is not described by an ideal neoclassical model.

IV. EFFECT OF FLUCTUATIONS ON THE PLASMA

Next, the role of fluctuations on confinement is examined. The experimental data presented indicate that fluctuations play an important role in EBT confinement. The stability criterion for interchange modes in the present EBT configuration is described and compared with measured pressure profiles. These considerations lead to the conclusion that the plasma is marginally stable for flute modes.

A. Density Fluctuations

One of the most important effects observed during the magnetic field scans is that the plasma fluctuation level increases significantly as the magnetic field is reduced. In order to quantify this effect, the line integral density fluctuations have been measured as a function of B using a 4-mm interferometer. The most interesting issue here is not the fluctuation level itself, but rather the correlation of the fluctuations with the plasma parameters. Percentage fluctuation levels ($\delta n_e \ell / n_e \ell$) for EBT-I and EBT-S are plotted in Fig. 5, together with the line integral density, as a function of the magnetic field. It is clear that the line integral density in both EBT-I and EBT-S decreases as the fluctuation level increases.

The frequency spectra for these fluctuations have been investigated, and the results are summarized in Fig. 6. The percentage fluctuation level in several frequency bands is plotted as a function of the magnetic field. The bandwidth (Δf) is 20 kHz. Although the low-frequency fluctuations

ORNL-DWG 84-3080R2 FED

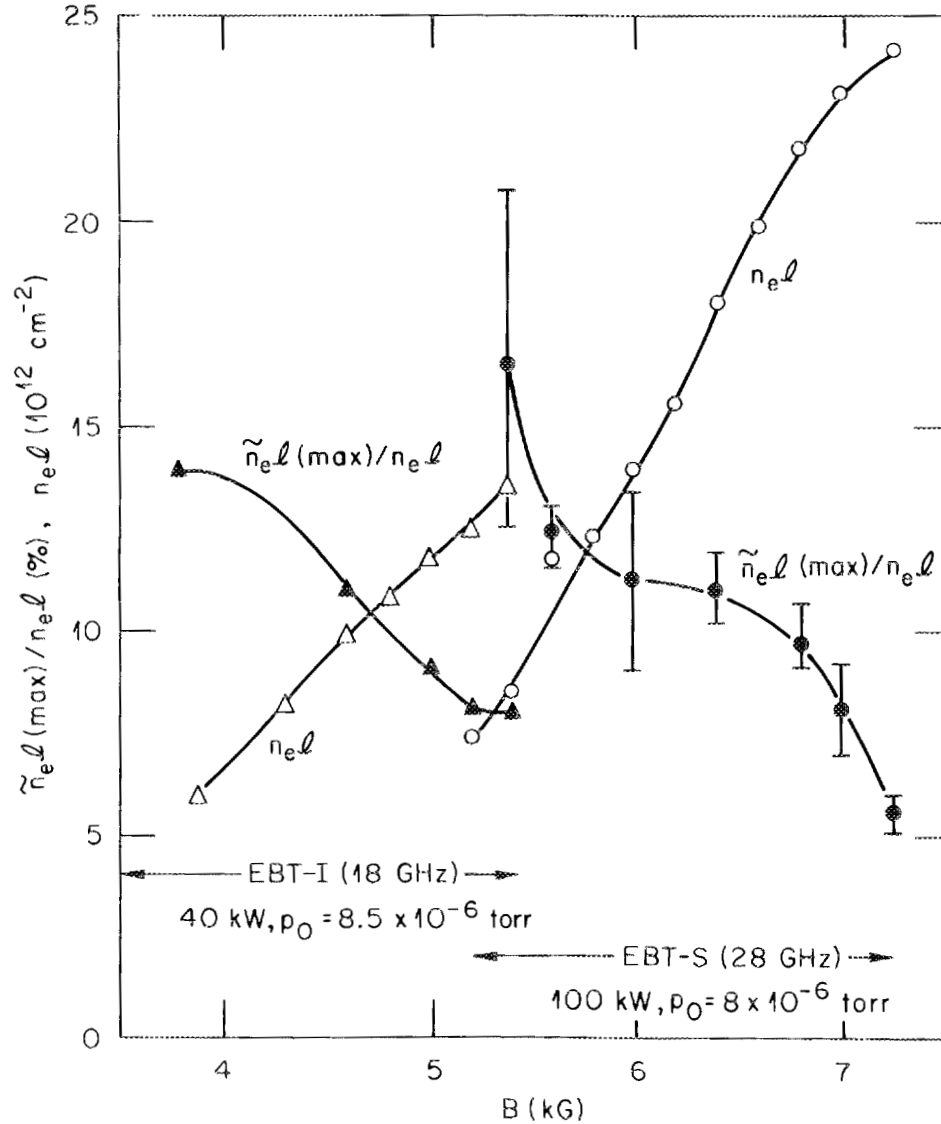


Fig. 5. Percentage density fluctuations (closed points) and line integral densities (open points) vs magnetic field strength. The standard field strength is 0.5 T in EBT-I and 0.725 T in EBT-S at the center of the midplane. The density fluctuations and the line integral densities change with the same trends. Heating frequencies are 18 GHz for EBT-I and 28 GHz for EBT-S.

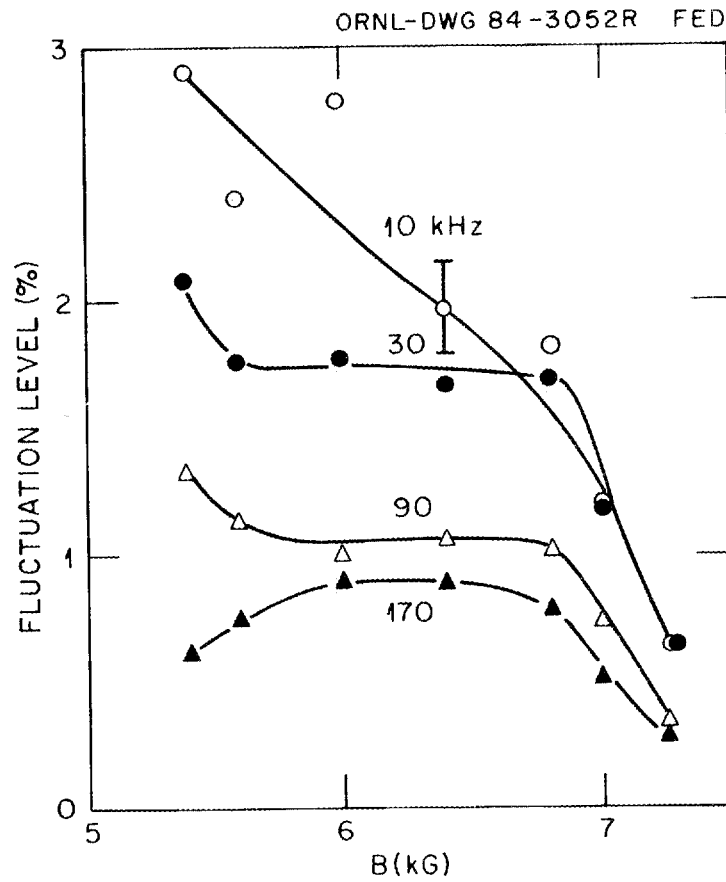


Fig. 6. Density fluctuation level (%) for different frequencies vs magnetic field strength. The bandwidth is +10 kHz. The microwave power is 100 kW, and the ambient pressure is 1×10^{-6} Torr.

($f \sim 10$ kHz) decrease monotonically with magnetic field, the fluctuations at higher frequencies exhibit a plateau for intermediate values of magnetic field, 0.58 to 0.68 T. Therefore, although the shape of the frequency spectra demonstrates a dependence on the magnetic field, in general the fluctuation level is a monotonically decreasing function of the frequency. What we have been examining here are variations of the background fluctuations that resemble broadband noise and are always present in EBT operation. These fluctuations are usually associated with C-mode operation but are also present throughout T-mode at a reduced level.

In several instances, coherent modes have been observed, superimposed upon the background fluctuation spectra. The frequency spectra of the density fluctuations for ring killer and T-mode operation are displayed in Fig. 7. In each photo, the ordinate is a linear scale with arbitrary units and the abscissa is 20 kHz/division. The upper photo shows the effect of the limiter on the 150-kHz fluctuations typically observed in low-pressure, T-mode operation. When the limiter is placed just outside the field line that is connected to the second harmonic resonance on the midplane, the coherent signal at 150 kHz clearly disappears. This mode was identified⁹ as a flute mode with azimuthal mode number $m = 10$ localized near or just outside of the hot electron annulus. The limiter may stabilize this mode by line tying.

In the lower and middle spectra, fluctuation spectra for normal T-mode operation and ring killer¹⁸ operation are compared. Two groups of coherent fluctuations, near 20 kHz and 60 kHz, are superimposed on the normal broadband fluctuation spectra typical of T-mode. In this case, the absolute fluctuation level with the ring killer is about twice that of the reference T-mode case. Correspondingly, the electron energy density measured during ring killer operation is reduced by roughly a factor of two.

ORNL-PHOTO 0001-85R FED

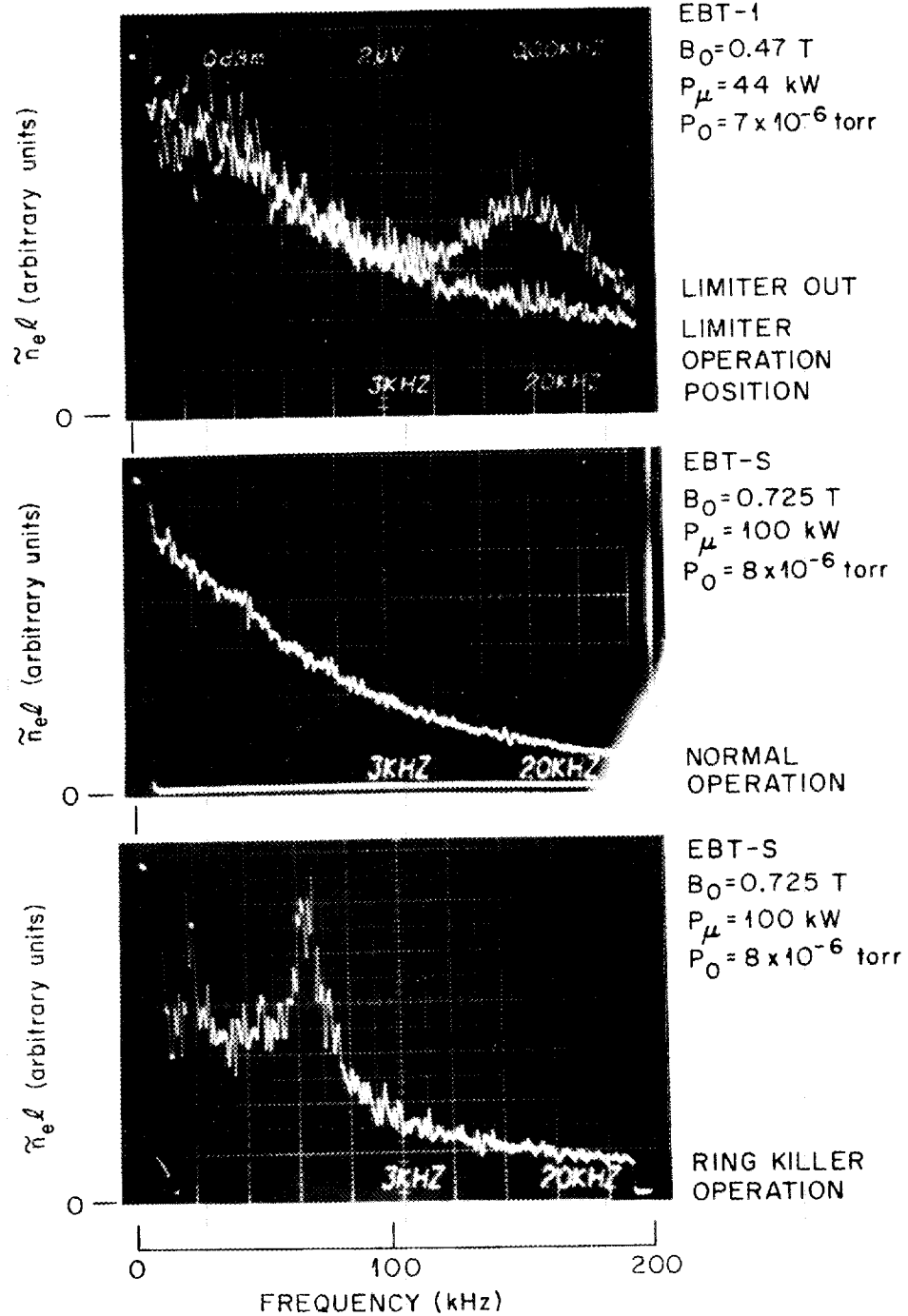


Fig. 7. The spectra of the density fluctuation for several different operations.

In order to quantify more clearly the magnitude of the coherent fluctuations relative to the broadband background fluctuations, the integrated fluctuation levels ($\int \delta n_e \ell / n_e \ell \, df$) of the two types of fluctuations can be compared. When this is done, it is found that the coherent modes are smaller by an order of magnitude for the two cases described above.

The most significant results from the fluctuation measurements can be summarized as follows:

1. Increases in the plasma parameters, specifically in line integral density and electron energy density, correlate well with percentage decreases in density fluctuation level for both EBT-I and EBT-S.
2. Generally, these fluctuations exhibit broadband noise-like behavior.
3. In some instances, coherent modes have been observed. However, their integrated fluctuation level is significantly smaller than that of the broadband background fluctuations.

B. Interchange Stability Criterion

A direct measurement of the magnetic field at the ring location has been carried out in the Nagoya Bumpy Torus (NBT)⁷ by using a neutral lithium beam and observing the Zeeman splitting of the electron-impact-excited lithium line spectrum. Ring beta was found to be about 6%. Measurements of the ring spatial profile in EBT⁸ show that the hot electron beta value is less than 10%. For both devices, this is not strong enough to reverse $\phi \, d\ell/B$. Therefore, the hypothesis that hot electron rings reverse the gradient of $\phi \, d\ell/B$ and provide gross MHD stability has not been experimentally realized in a bumpy torus. The following question can be raised: What kind of mechanism of gross stability sustains the plasma in EBT? In this regard, it is noted that

several stabilizing mechanisms have been proposed recently, including charge uncovering for flute modes¹⁹ and $\mathbf{E} \times \mathbf{B}$ velocity shear stabilization of drift waves.²⁰

The approach followed here is to re-examine the question of interchange stability for the situation where the ring beta is small and can be neglected; that is, the vacuum field configuration. The energy criterion¹⁰ of interchange modes can be expressed as

$$\delta W = p \delta U \delta[\ell n(pU^\gamma)] > 0, \quad (1)$$

where δW is the change in plasma energy, p is the plasma pressure, U is the flux tube volume ($= \oint d\ell/B$), and γ is the ratio of specific heats. For the case of EBT, $\delta U > 0$ everywhere on the radial profile, and the energy criterion reduces to the so-called compressibility criterion²¹

$$\delta(\ell n pU^\gamma) > 0. \quad (2)$$

The radial plasma pressure profiles that are consistent with the interchange stability can then be predicted on the basis of this expression. If the pressure profile is compared with the profile of $U^{-\gamma}$, the criterion is satisfied whenever the pressure profile is flatter (broader) than the $U^{-\gamma}$ profile. Although such a condition is tenable in the interior of the plasma, the edge region, where the pressure must eventually drop to zero, presents a problem. In EBT, however, line tying of field lines to the cavity walls provides a mechanism for stabilizing flute modes in the surface plasma region ($16 \text{ cm} < r < 25 \text{ cm}$). Thus, the interior of the plasma can be interchange stable, provided that the pressure profile is not so steep as to violate the compressibility criterion, and the plasma edge can be stabilized by line tying. Nevertheless, it is apparent that this places a significant restriction on the plasma pressure profile. Any natural tendency of the plasma toward a profile that is more peaked than that

allowed by the compressibility criterion results in a marginally unstable plasma.

C. Discussion of the Stability of the Interchange Mode (Coherent Mode)

On the basis of the preceding discussion, it is of interest to compare the plasma pressure profiles in EBT with the calculated profiles of U^γ . For this purpose, the Thomson scattering measurements of electron density and temperature at $r = 0$ and at $r = 8$ cm are used. Because the ion temperature is quite low, the ion contribution to the plasma pressure will be neglected. The plasma pressure ratio at $r = 0$ and $r = 8$ cm, as shown in Fig. 1, is examined using Eq. (2). For these two points, the stability condition is written as

$$p(r=8) U^\gamma(r=8) - p(r=0) U^\gamma(r=0) \geq 0$$

or

$$\frac{p(r=8)}{p(r=0)} \geq \frac{U^\gamma(r=0)}{U^\gamma(r=8)}$$

The pressure ratio $p(8)/p(0)$ is presented in Fig. 8 as a function of the magnetic field. The experimental data are compared with marginal stability lines, given by the ratio $U^\gamma(0)/U^\gamma(8)$, obtained from a three-dimensional numerical calculation of U . Because of the uncertainty in the correct value of γ , three marginal stability lines are provided in Fig. 8. The proper choice of γ is determined by the number of degrees of freedom of the confined particles. In the case of EBT, the U profile and γ should be determined by a drift-orbit weighting of the trapped and passing particle distributions. This calculation

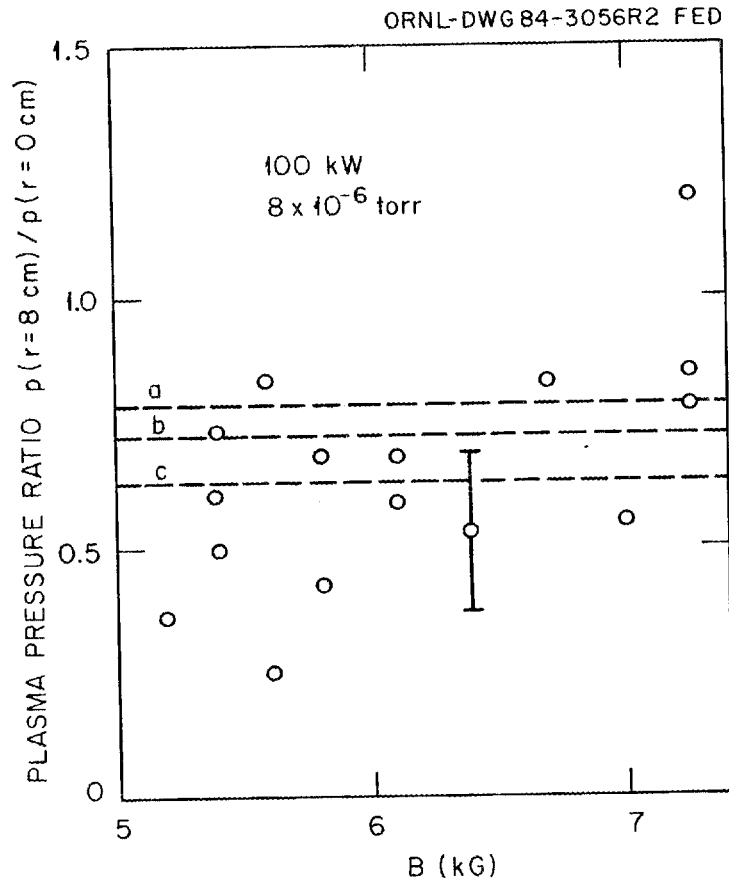


Fig. 8. The plasma pressure ratios between $r = 0$ and $r = 8$ cm vs magnetic field strength. The three lines correspond to (a) $U^\gamma(r = 0)/U^\gamma(r = 8 \text{ cm})$ with $\gamma = 1.5$, (b) $\gamma = 2.0$, and (c) $B^2(r = 0)/B^2(r = 8)$.

has not been done. The values chosen, $\gamma = 1.5$ and $\gamma = 2$, are representative of particle distributions with approximately two and three degrees of freedom respectively. The third line, motivated by considerations of a simple evaluation of the stability criterion, shows the ratio $[B(8)/B(0)]^2$ obtained using midplane values of the magnetic field.

When the data of Figs. 7 and 8 are evaluated in detail, it is found that the pressure profile (Fig. 8) is more or less flat within the uncertainty of the data as shown by the error bar, except for high and low magnetic field operation. It seems reasonable to conclude that the plasma in the present EBT configuration is marginally stable, being governed by the compressibility criterion, Eq. (2). Basically, the observation of coherent modes (Fig. 7) tends to support this viewpoint. The coherent flute modes at 150 kHz tend to occur for low-pressure operation, precisely where the pressure profile tends to be most peaked. It is anticipated that the ring killers lower the plasma pressure in the edge region and steepen the profile just inside the limiter position ($r \approx 12$ cm). Therefore, the observation of large-amplitude coherent modes, at 20 and 60 kHz, for such conditions is not unexpected.

D. Correlation of Background Noise with Plasma Parameters

As mentioned in Sec. IV.A, the integrated fluctuation level ($\int \delta n_e \ell df$) is much larger than that of any coherent mode. Except for extreme cases such as low-pressure T-mode or low magnetic field operation, violent fluctuations are not found in the EBT plasma. The interesting issue is the importance of the background fluctuations for confinement.

Figures 3 and 5 clearly show that the line integral density and/or the bulk electron stored energy increase as the density fluctuation level decreases. The result, a line integral density in EBT-I at $B = 0.54$ T that is

60% higher than that in EBT-S (with ECH power in EBT-S 2.5 times that in EBT-I), supports the hypothesis that the background noise is very important for confinement.

Another interesting result is found when the fluctuation level, the electron stored energy, and the power flow to the limiter are examined. The limiter is installed just outside the magnetic field line of the second cyclotron harmonic at the midplane in the case of $B = 0.725$ T and is used to measure the power flow. From the limiter measurement, 20% of the power absorbed by the bulk plasma goes around the torus. This circulating power correlates strongly with the fluctuations, as shown in Fig. 9.

When the magnetic field strength is increased, the plasma energy density increases as B^2 , but the limiter power decreases. Generally, the energy density W_e , the limiter power P_ℓ , and the diffusion coefficient D_e may be related by

$$P_\ell \sim W_e D_e / a^2 ,$$

where a is the plasma radius. When D_e is proportional to $(\delta n_e \ell / n_e \ell)^2$, D_e increases as B decreases. The experimental results shown in Fig. 9 are qualitatively consistent with this anomalous transport, which is also indicated in Sec. III.

In summary, it is found that fluctuations are quite important to the understanding of transport in EBT. The electron energy density is shown to be inversely related to the percentage fluctuation level. The broadband noise-like background fluctuations appear to be more important due to their larger total fluctuation amplitude. A comparison of the plasma pressure profile with a calculation of U indicates that, in general, the plasma in the present EBT

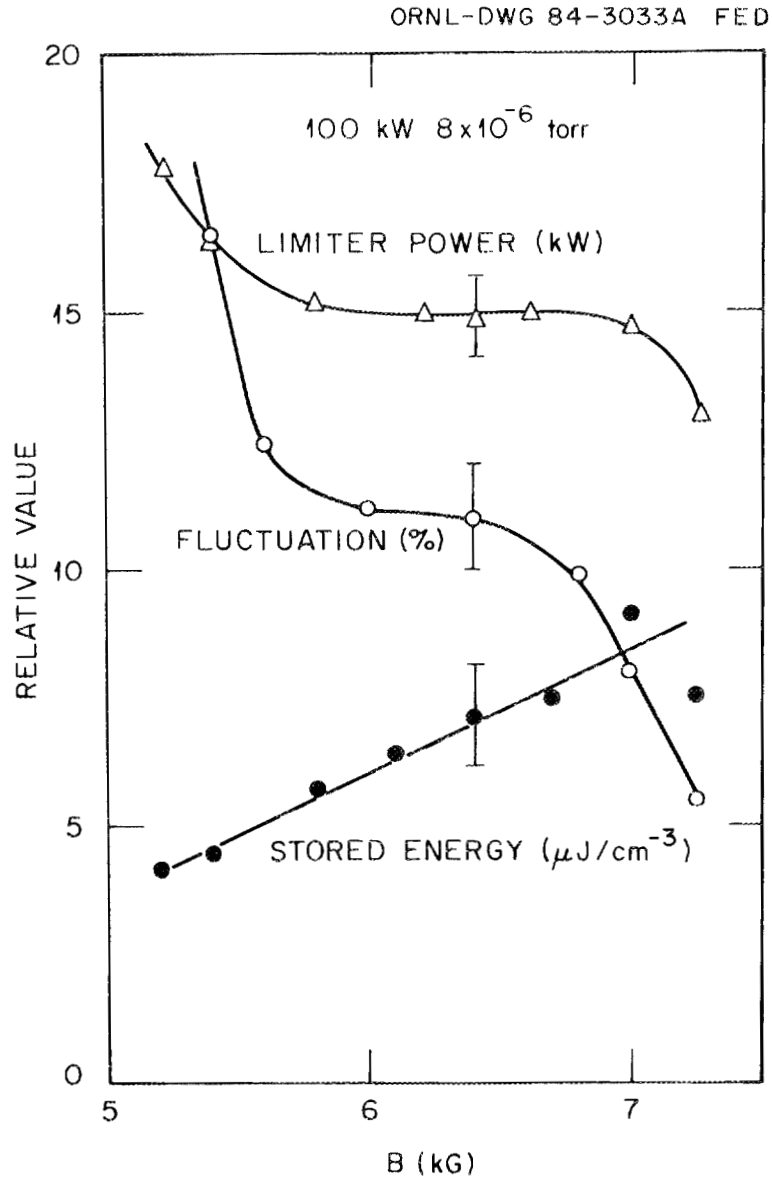


Fig. 9. The stored energy at the machine center, the power flow into the limiter, and the percentage fluctuation level vs the magnetic field strength.

configuration is probably marginally stable with respect to interchange modes. In fact, for operating conditions that tend to favor more peaked pressure profiles, coherent flute modes are observed.

V. SCALING OF PLASMA PARAMETERS

As mentioned previously, the plasma parameters do not strongly depend on the radial electric field strength, and it is likely that the plasma is marginally stable. These observations make neoclassical scaling arguments questionable, and a lack of detailed knowledge of the anomalous transport mechanism for EBT makes discussions of plasma confinement difficult. One convenient method for discussing the EBT confinement properties is to plot the plasma density n_e as a function of the electron temperature T_e for different plasma conditions, as shown in Fig. 10.

Data are included for (1) a normal pressure scan (with open squares for data obtained in the C-mode and open circles for data measured in the T-mode); (2) ring killer¹⁴ operation (closed circles); (3) "ring modifier"¹⁴ operation (closed triangles); and (4) a magnetic field scan (closed squares), where the magnetic field strengths are indicated near each data point. The short-dashed line for the pressure scan is drawn from the product of the best fit of n_e and T_e on the raw data. In Fig. 10 the data points are also compared with the solid curves with $3/2(n_e T_e) = \text{const.}$

The interesting trends found in compilation of these data sets are summarized as follows:

1. The electron density (n_e) generally decreases as the temperature (T_e) increases.
2. In the C-mode for a normal pressure scan (150 kW), the data points lie on the line of $3/2(n_e T_e) = 4.5 \times 10^{13} \text{ eV-cm}^{-3}$ (n_e is inversely proportional to

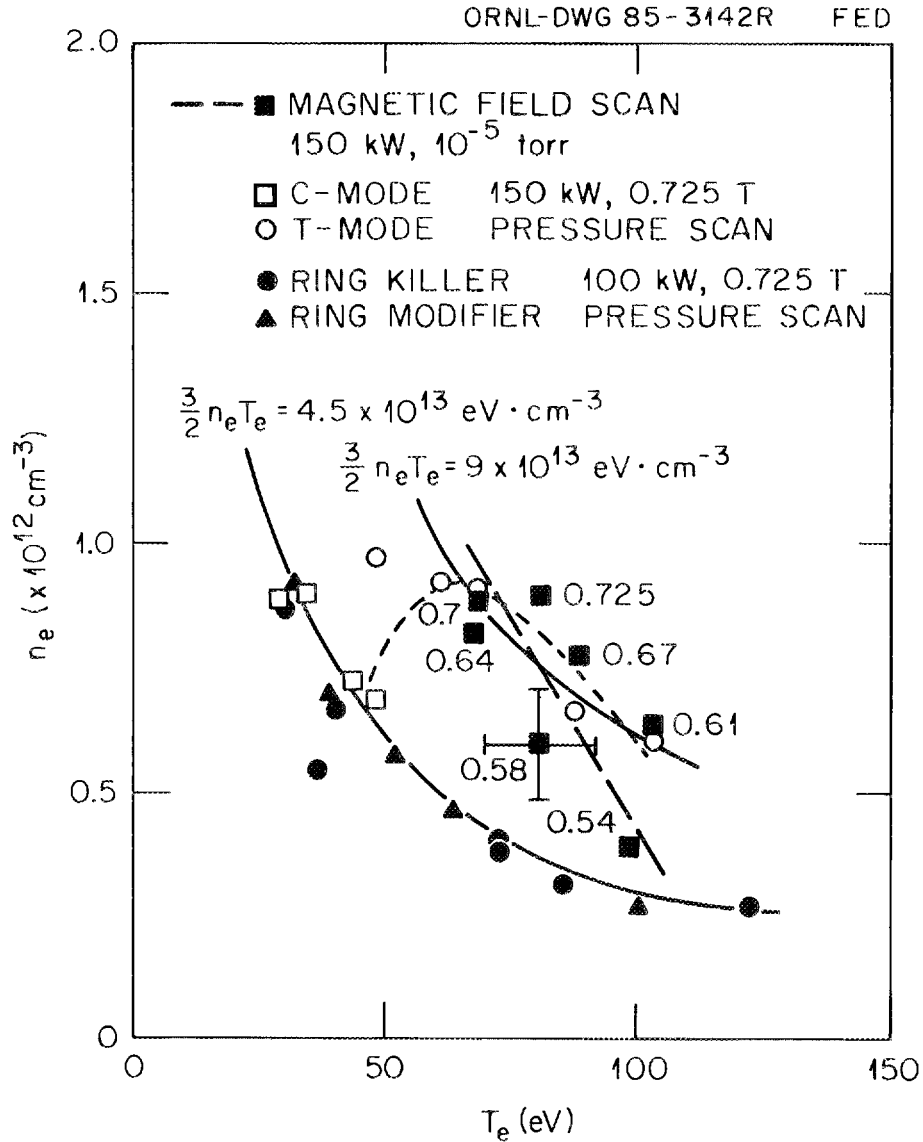


Fig. 10. Density n_e vs temperature T_e for different operation modes. Data are measured with the Thomson scattering technique at $r = 0$ cm. The magnetic field scan (■) and the pressure scan (□ and ○) were carried out with $P_{\mu} = 150$ kW. Ring killer (●) and modifier (▲) data are from experiments with $P_{\mu} = 100$ kW. The magnetic field scan data are labeled with field strength.

T_e). In the case of ring killer and ring modifier during 100-kW operation, n_e is also inversely proportional to T_e , and $3/2(n_e T_e)$ lies on the same line as the C-mode for the two powers.

3. In the T-mode at higher ambient pressure, lower T_e is observed, and n_e increases as T_e increases. This is clear in the case of the dotted line (best fit of raw data). This is quite attractive. In the T-mode at lower ambient pressure, n_e is again inversely proportional to T_e . The product of $n_e T_e$ is larger than the constant in the C-mode and in the ring killer case.
4. The data points obtained from the magnetic field scan are observed to move from the lower $n_e T_e$ line (C-mode and ring killer) to the higher $n_e T_e$ line as the magnetic field increases from 0.54 T to 0.725 T.

Figure 2 can be related to Fig. 10 as an operational trajectory that takes the plasma from the lower limit to the upper limit. This can be seen by taking the mirror image of Fig. 2 and by noting that both ordinates represent density and both abscissas represent electron temperatures. As the ambient pressure is reduced, the electron temperature increases.¹³ The data for the pressure scan at $B = 0.52$ T in Fig. 2 lie on an extended line of the C-mode in the normal operation. The data for $B = 0.54$ T in Fig. 10 also lie on the extension line of the C-mode and on the ring killer line. The plasma in the C-mode is not in equilibrium, and the plasma under the ring killer is unstable. The plasma in the lower magnetic field is therefore either not in equilibrium or unstable. This operation ($B = 0.52$ T) may represent a base case for EBT operation. The magnetic field scan covers the whole operation regime in EBT from the base case to the normal case. Therefore, Fig. 2 indicates the EBT confinement properties, qualitatively.

The product of $n_e T_e$ is constant when high levels of fluctuations are present ($\delta n_e \ell / n_e \ell \approx 15\%$, C-mode, ring killer case, and hot-electron

instability) and/or in nonequilibrium (C-mode). The lower value of the product $n_e T_e$ is not a function of the heating power. This value is expressed empirically,

$$3/2(n_e T_e) \approx 4.5 \times 10^{13} \text{ eV-cm}^{-3}$$

The upper limit of the product $n_e T_e$ is written by

$$3/2(n_e T_e) \approx 9.0 \times 10^{13} \text{ eV-cm}^{-3}$$

in the case of 150 kW. The constant of the upper limit may have a power dependence because the product $3/2(n_e T_e)$ at 100 kW is $7 \times 10^{13} \text{ eV-cm}^{-3}$.

VI. CONCLUSION

We have discussed experimentally whether the plasma parameters of EBT obey the neoclassical transport or the anomalous transport. The comparison of plasma parameters with changes in the potential profile indicates that the electron energy densities do not scale with collisionless neoclassical transport $(E/T_e)^2$. They correlate well with the percentage density fluctuation level. The gross stability condition is marginally satisfied with the governing criterion of $\delta(\ln pU^{\nu}) > 0$ for flute modes. When the pressure profile becomes steeper than the U^{ν} profile, density fluctuations of coherent modes are active. The electron energy density decreases as the broadband noise increases rather than with an increase in coherent mode amplitude.

The plasma stored energy density $[3/2(n_e T_e)]$ for the bulk component is restricted between the following values in the case of 100 kW:

$$4.5 \times 10^{13} \text{ eV-cm}^{-3} < 3/2(n_e T_e) < 7 \times 10^{13} \text{ eV-cm}^{-3}$$

The lower limit does not depend on the heating power and is associated with a nonequilibrium state and/or low-frequency instabilities. The upper

limit is phenomenologically related to hot-electron instabilities. The value of the upper limit appears to depend somewhat on heating power.

An attractive pressure region is found where the electron density increases as the electron temperature increases. This implies that the stabilization of the hot-electron modes is an important issue for improving the plasma parameters in this type of confinement system.

VII. ACKNOWLEDGMENTS

The authors would like to express their appreciation to the members of the EBT operation group for their technical support in these experiments.

REFERENCES

1. R. A. Dandl, H. O. Eason, A. C. England, G. E. Guest, C. L. Hedrick, J. C. Sprott, ORNL/TM-3694, Oak Ridge National Laboratory, 1971; R. A. Dandl, H. O. Eason, A. C. England, G. E. Guest, C. L. Hedrick, H. Ikegami, and D. B. Nelson, in Plasma Physics and Controlled Nuclear Fusion Research 1974 (IAEA, Vienna, 1975), Vol. II, p. 141.
2. E. F. Jaeger, D. A. Spong, and C. L. Hedrick, Phys. Rev. Lett. **40**, 866 (1978).
3. D. B. Nelson and C. L. Hedrick, Nucl. Fusion **19**, 283 (1979).
4. F. M. Bieniosek and K. A. Connor, Phys. Fluids **26**, 2256 (1983).
5. T. Uckan, L. A. Berry, D. L. Hillis, and R. K. Richards, Phys. Fluids **25**, 1253 (1982); D. L. Hillis, G. R. Haste, and L. A. Berry, Phys. Fluids **26**, 820 (1983); D. E. Hastings, Phys. Fluids **27**, 2272 (1984).
6. S. Hiroe, J. A. Cobble, R. J. Colchin, G. L. Chen, K. A. Connors, J. R. Goyer, and L. Solensten, to be published in Phys. Fluids.
7. K. Kadota, C. Takahashi, H. Iguchi, M. Fujiwara, K. Matsunaga, and J. Fujita, Rev. Sci. Instrum. **56**, 857 (1985).
8. D. L. Hillis, J. B. Wilgen, T. S. Bigelow, E. F. Jaeger, D. W. Swain, O. E. Hankins, and R. Juhala, to be published in Phys. Fluids.
9. A. Komori, Nucl. Fusion **24**, 1173 (1984).
10. M. N. Rosenbluth and C. L. Longmire, Ann. Phys. **1**, 120 (1957).
11. J. C. Glowienka, J. Vac. Sci. Technol. **18**, 1088 (1981).
12. L. Solensten, Rensselaer Polytechnic Institute, private communication, 1984.
13. J. A. Cobble, Rev. Sci. Instrum. **56**, 73 (1985).

14. The ring killer is an array of 24 small limiters that are inserted in the hot electron annulus to destroy the hot electron population. Ring modifiers are installed at 5 cm radially outside the ring. They do not extend fully into the ring and only decrease the hot electron population. See also Ref. 18.
15. S. Hiroe, J. B. Wilgen, F. W. Baity, L. A. Berry, R. J. Colchin, W. A. Davis, A. M. El Nadi, G. R. Haste, D. L. Hillis, T. L. Owens, D. A. Spong, and T. Uckan, Phys. Fluids **27**, 1019 (1984).
16. N. G. Popkov, Fiz. Plazmy **5**(4), 482 (1979) [Sov. J. Plasma Phys.].
17. A. M. El Nadi, Phys. Fluids **28**, 878 (1985).
18. D. L. Hillis, J. B. Wilgen, J. A. Cobble, S. Hiroe, W. A. Davis, D. A. Rasmussen, R. K. Richards, T. Uckan, E. F. Jaeger, O. E. Hankins, J. R. Goyer, and L. Solensten, Phys. Fluids **28**, 2848 (1985).
19. D. A. Spong, Charge Uncovering Effects on Flute Instabilities in Hot Electron Plasmas, ORNL/TM-9420, Oak Ridge National Laboratory, 1985.
20. H. Sanuki, Phys. Fluids **27**, 2500 (1984).
21. J. R. Ferron, A. Y. Wong, G. Dimonte, and B. J. Leikind, Phys. Fluids **26**, 2227 (1983).

INTERNAL DISTRIBUTION

- | | |
|-----------------------|--|
| 1. F. W. Baity | 25. R. K. Richards |
| 2. D. B. Batchelor | 26. J. Sheffield |
| 3. L. A. Berry | 27. D. A. Spong |
| 4. T. S. Bigelow | 28. D. W. Swain |
| 5. W. H. Casson | 29. J. S. Tolliver |
| 6-7. G. L. Chen | 30. N. A. Uckan |
| 8. R. J. Colchin | 31. T. Uckan |
| 9-10. J. C. Glowienka | 32. T. L. White |
| 11. G. R. Haste | 33-34. J. B. Wilgen |
| 12. C. L. Hedrick | 35-36. Laboratory Records Department |
| 13-14. D. L. Hillis | 37. Laboratory Records, ORNL-RC |
| 15-19. S. Hiroe | 38. Document Reference Section |
| 20. E. F. Jaeger | 39. Central Research Library |
| 21. H. D. Kimrey | 40. Fusion Energy Division Library |
| 22. L. W. Owen | 41-42. Fusion Energy Division Publications
Office |
| 23. T. L. Owens | 43. ORNL Patent Office |
| 24. D. A. Rasmussen | |

EXTERNAL DISTRIBUTION

44. Office of the Assistant Manager for Energy Research and Development, U.S. Department of Energy, Oak Ridge Operations, P.O. Box E, Oak Ridge, TN 37831
- 45-46. J. A. Cobble, Los Alamos National Laboratory, Los Alamos, NM 87545
- 47-48. A. M. El Nadi, Cairo University, Giza, Egypt
- 49-50. J. R. Goyer, Rensselaer Polytechnic Institute, 110 Eighth St., Troy, NY 12181
- 51-52. L. Solensten, Rensselaer Polytechnic Institute, 110 Eighth St., Troy, NY 12181
- 53-54. W. H. Casson, The University of Tennessee, Knoxville, TN 37916
- 55-56. O. E. Hankins, University of North Carolina at Raleigh, Raleigh, NC 27695-7909
- 57-58. B. H. Quon, JAYCOR, 11011 Torreyana Rd., P.O. Box 85154, San Diego, CA 92138
59. J. M. Turner, Mirror Systems Branch, Office of Fusion Energy, Office of Energy Research, Mail Stop G-256, U.S. Department of Energy, Washington, DC 20545
60. M. Fujiwara, Institute of Plasma Physics, Nagoya University, Nagoya 464, Japan
61. T. V. George, Office of Fusion Energy, Office of Energy Research, Mail Station G-256, U.S. Department of Energy, Washington, DC 20545

62. T. Shoji, Institute of Plasma Physics, Nagoya University, Nagoya 464, Japan
63. A. Komori, Interdisciplinary Graduate School of Engineering Sciences, Kyushu University, Kasuga, Fukuoka 816, Japan
64. N. A. Krall, JAYCOR, 11011 Torreyana Rd., P.O. Box 85154, San Diego, CA 92138
65. S. Hamasaki, JAYCOR, 11011 Torreyana Rd., P.O. Box 85154, San Diego, CA 92138
66. N. H. Lazar, TRW Defense and Space Systems, 1 Space Park, Bldg. R-1, Redondo Beach, CA 92078
67. J. B. McBride, Science Applications, Inc., 1200 Prospect St., P.O. Box 2351, La Jolla, CA 92037
68. W. B. Ard, McDonnell Douglas Astronautics Company, Bldg. 278, P.O. Box 516, St. Louis, MO 63166
69. H. L. Berk, Institute of Fusion Studies, University of Texas at Austin, Robert L. Moore Hall, Rm. 11.218, Austin, TX 78712
70. F. M. Bieniosek, McDonnell Douglas Astronautics Company, Bldg. 278, P.O. Box 516, St. Louis, MO 63166
71. R. A. Dandl, Applied Microwave Plasma Concepts, 2210 Encinitas Blvd., Suite P, Encinitas, CA 92024
72. R. S. Post, Plasma Fusion Center, Massachusetts Institute of Technology, 190 Albany St., Cambridge, MA 02139
73. D. H. McNeill, Plasma Physics Laboratory, Princeton University, P.O. Box 451, Princeton, NJ 08544
74. K. Mizuno, Applied Science Dept., University of California—Davis, 228 Walker Hall, Davis, CA 95617
75. F. L. Ribe, College of Engineering, AERL Building, FL-10, University of Washington, Seattle, WA 98195
76. T. C. Simonen, Lawrence Livermore National Laboratory, P.O. Box 808, Livermore, CA 94550
77. H. Weitzner, Courant Institute of Mathematical Sciences, New York University, 251 Mercer St., New York, NY 10012
78. K. Tsang, Science Applications, Inc., 934 Pearl St., Boulder, CO 80302
79. B. Fried, Department of Physics, University of California, Los Angeles, CA 90024
80. J. W. Van Dam, Institute for Fusion Studies, University of Texas at Austin, Austin, TX 78712
81. A. Wong, Department of Physics, University of California, Los Angeles, CA 90024
82. H. Goede, R1/2144, TRW Inc., Energy Development Group, One Space Park, Redondo Beach, CA 90278
83. H. K. Forsen, Bechtel Group, Inc., Research Engineering, P.O. Box 3965, San Francisco, CA 94105
84. J. R. Gilleland, GA Technologies, Inc., Fusion and Advanced Technology, P.O. Box 81608, San Diego, CA 92138
85. R. A. Gross, Plasma Research Laboratory, Columbia University, New York, NY 10027
86. D. M. Meade, Princeton Plasma Physics Laboratory, P.O. Box 451, Princeton, NJ 08544

87. F. Prevot, CEN/CADARACHE, Department de Recherches sur la Fusion Controllee, 13108 Saint-Paul-Lez-Durance, Cedex, France
88. M. Roberts, International Programs, Office of Fusion Energy, Office of Energy Research, ER-52 Germantown, U.S. Department of Energy, Washington, DC 20545
89. W. M. Stacey, School of Nuclear Engineering, Georgia Institute of Technology, Atlanta, GA 30332
90. D. Steiner, Rensselaer Polytechnic Institute, Nuclear Engineering Department, NES Building, Tibbets Avenue, Troy, NY 12181
91. R. Varma, Physical Research Laboratory, Navrangpura, Ahmedabad 380009, India
92. R. W. Conn, Department of Chemical, Nuclear, and Thermal Engineering, University of California, Los Angeles, CA 90024
93. J. D. Callen, Department of Nuclear Engineering, University of Wisconsin, Madison, WI 53706
94. D. D. Ryutov, Institute of Nuclear Physics, Siberian Branch of the Academy of Sciences of the U.S.S.R., Sovetskaya St. 5, 630090 Novosibirsk, U.S.S.R.
95. S. O. Dean, Director, Fusion Energy Development, Science Applications, Inc., 2 Professional Drive, Gaithersburg, MD 20760
96. G. A. Eliseev, I. V. Kurchatov Institute of Atomic Energy, P.O. Box 3402, 123182 Moscow, U.S.S.R.
97. V. A. Glukhikh, Scientific-Research Institute of Electro-Physical Apparatus, 188631 Leningrad, U.S.S.R.
98. N. A. Davies, Office of Fusion Energy, Office of Energy Research, Mail Stop G-256, U.S. Department of Energy, Washington, DC 20545
99. G. Gibson, Westinghouse Electric Corporation, Fusion Power Systems Department, P.O. Box 10864, Pittsburgh, PA 15236
100. R. W. Gould, Department of Applied Physics, California Institute of Technology, Pasadena, CA 91109
101. D. G. McAlees, Exxon Nuclear Company, Inc., 2101 Horn Rapids Road, Richland, WA 99352
102. J. F. Clarke, Associate Director for Fusion Energy, Office of Energy Research, Office of Fusion Energy, Department of Energy, Mail Station G-256, Washington, DC 20545
103. D. B. Nelson, Acting Director, Division of Applied Plasma Physics, Office of Fusion Energy, Office of Energy Research, Mail Stop G-256, U.S. Department of Energy, Washington, DC 20545
104. Documentation S.I.G.N., Departement de la Physique du Plasma et de la Fusion Controllee, Centre d'Etudes Nucleaires, B.P. No. 85, Centre du Tri, 38041 Cedex, Grenoble, France
105. Bibliotheque, Service du Confinement des Plasmas, CEA, B.P. 6, 92 Fontenay-aux-Roses (Seine), France
106. Bibliothek, Institut fur Plasmaphysik, KFA, Postfach 1913, D-5170 Julich, Federal Republic of Germany
107. Bibliothek, Max-Planck Institut fur Plasmaphysik, D-8046 Garching bei Munchen, Federal Republic of Germany
108. Bibliotheque, Centre de Recherches en Physique des Plasmas, 21 Avenue des Bains, 1007 Lausanne, Switzerland

109. Library, Culham Laboratory, UKAEA, Abingdon, Oxfordshire, OX14 3DB, England
110. Library, FOM Instituut voor Plasma-Fysica, Rijnhuizen, Edisonbaan 14, 3439 MN Nieuwegein, The Netherlands
111. Library, Institute of Physics, Academia Sinica, Beijing, Peoples Republic of China
112. Library, Institute of Plasma Physics, Nagoya University, Nagoya 64, Japan
113. Library, International Centre for Theoretical Physics, Trieste, Italy
114. Library, Laboratorio Gas Ionizzati, I-00044 Frascati, Italy
115. Library, Plasma Physics Laboratory, Kyoto University, Gokasho, Uji, Kyoto, Japan
116. Plasma Research Laboratory, Australian National University, P.O. Box 4, Canberra, A.C.T. 2000, Australia
117. Thermonuclear Library, Japan Atomic Energy Research Institute, Tokai, Naka, Ibaraki, Japan
- 118-309. Given distribution as shown in TID-4500, Magnetic Fusion Energy (Category UC-20 f,g: Theoretical Plasma Physics and Experimental Plasma Physics)